Optimal Electric-Distribution-Grid Planning considering the Demand-Side Flexibility of Thermal Building Systems for a Test Case in Singapore

Sebastian Troitzsch[a,*], Bhargava Krishna Sreepathi[c], Thanh Phong Huynh[a], Aurelie Moine[a], Sarmad Hanif[b], Jimeno Fonseca[c], Thomas Hamacher[d]

[a] *TUMCREATE, Singapore*
[b] *Pacific Northwest National Laboratory, USA*
[c] *Singapore-ETH Centre, Singapore*
[d] *Technical University of Munich (TUM), Germany*

Abstract

The planning of electric distribution grids aims at designing the most cost-efficient grid topology, while ensuring sufficient maximum capacity in the case of peak load conditions. With the advent of demand side flexibility, there is the opportunity to reshape peak loads such that the investment cost of the electric grid decreases, in exchange for a minor increase in the operating cost. To this end, there exists a gap in formulating the trade-off between investment cost and operating cost, and a unsatisfactory understanding of the potential cost savings. This paper formulates a numerical optimization problem for the planning of the electric distribution grid, which incorporates the demand side flexibility from thermal building systems, e.g., heating, ventilation and air-conditioning systems. The problem is formulated as a single-stage, mixed-integer quadratic program and aims at minimizing the investment cost for the grid along with the operating cost of the flexible loads. This is subject to the fixed electricity demand and thermal-comfort constraints of building occupants. The approach is tested on a district planning test case based in Singapore, where the results show reductions of up to 36.3 % in investment cost and reductions of up to 0.81 % in total annualized cost. Urban planning authorities, developers and utility companies can all benefit from the presented approach to make optimized investment decisions. For building operators, the results point to the need to adopt control systems for demand side flexibility.

Keywords: Demand Side Flexibility, Power System Planning, Optimal Planning and Operation

1. Introduction

Electric-distribution-grid planning, i.e., power system planning, aims at designing a grid topology which is cost-efficient, and yet ensures sufficient maximum capacity in the case of peak load conditions. The maximum capacity of the electric grid is constrained by 1) the thermal limits of the grid equipment, i.e., the maximum current which can be carried without causing damage, and 2) the voltage limits, i.e., the voltage range at which the electric devices of customers can operate. The peak load conditions can be characterized by the maximum coincident demand of the electric customers in the distribution grid, which can be inferred through load surveys [1]. However, the peak load does not usually take electric demand-side flexibility (DSF) into account, which can enable electric customers to shave their maximum demands.

DSF has first gained attention as a tool for balancing renewable generation [2, 3]. In particular, DSF helps to match generation and demand by shifting flexible loads to time periods with high renewable generation [2]. This helps in the avoidance of renewable generation shedding. In a microgrid, this can also help to decrease the need for additional energy storage systems, because a higher share of renewable electricity is instantly consumed [3]. DSF can also ensure that electric grid constraints are maintained throughout the operation [4] or they can support the grid stability by offering reserves [5]. Hence, the integration of the electric planning problem with DSF may thus reduce the required maximum capacity of the electric grid.

Thermal building systems, e.g., HVAC systems, are important candidates for DSF as they account for a large share of the electricity demand in buildings, particularly in tropical cities such as Singapore [6]. DSF from HVAC systems has seen increased attention with the advances in model predictive control (MPC) applications for buildings [7]. With MPC, the control problem of the HVAC system is expressed as a numerical optimization problem aimed at minimizing the building operating cost, i.e., the cost for consuming energy, while satisfying the occupant comfort constraints, i.e., the acceptable limits for indoor air temperature and indoor air quality. The building operator benefits from MPC through cost savings which arise from 1) more energy efficient control and 2) the ability to take dynamic electricity tariffs into account [8], i.e., the electric demand is shifted to hours with low electricity prices. This paper aims to integrate DSF into the planning of electric grids at the district scale.

In the planning of electric grids, i.e., power system plan-

*Corresponding author
Email address: sebastian.troitzsch@tum-create.edu.sg (Sebastian Troitzsch)

ning, there has been increased attention for approaches based on numerical optimization [9, 10]. The electric grid planning problem can be expressed as a numerical optimization problem for the minimization of the investment cost, i.e., the acquisition and installation costs of electric grid equipment, while ensuring peak load satisfaction and the electric grid constraints, i.e., thermal limits and voltage limits. However, these approaches do not yet consider DSF and its ability to reduce peak loads. Similarly, investment and unit-commitment strategies for electricity generation plants often consider the electric grid constraints to assess the grid-hosting capacity [11], but do not consider investment decisions in options around expanding the electric grid. Other tools for the planning and operation of multi-energy systems [12] focus on the optimal utilization of energy resources, but only consider rudimentary grid-expansion strategies rather than complete green-field planning strategies for the district scale. In [13], a multi-stage optimization methodology is proposed for the expansion of the electric distribution grid, combined with the deployment of distributed generation, but the work does not consider DSF. Further works have focused on the optimal operation, i.e., dispatch, of flexible resources subject to electric grid constraints [4, 14, 15]. In [4, 14], distributed optimization problems are proposed, where power limits [4] or nodal price increases [14] are imposed such that flexible loads are forced to respect the electric-grid constraints. In [15] a scheme is developed in which flexible loads are centrally dispatched to follow a pre-defined demand schedule. However, none of the works [4, 14, 15] include the planning of electric grids.

This paper aims at integrating the planning of electric grids and the operation of thermal building systems on a district scale, with the goal of reducing the maximum electric grid capacity requirement by considering the peak shaving capabilities due to DSF. The outcome of the combined planning and operation problem is studied for a test case in Singapore, and the distribution of investment cost and operating cost is highlighted along with the eventual cost savings. To this end, the results provide valuable insights for urban planning authorities, developers and utility companies in terms of how to optimize their investment decisions.

The integrated problem is formulated as an optimization problem which aims at minimizing the investment cost of the electric grid, along with the cost of losses in the electric grid and the operating cost of the thermal building systems, subject to the electric-grid constraints and the occupancy-comfort constraints. In a similar fashion, [16] proposed an optimization-based methodology for the integrated planning and operation of building energy systems, which was proposed through a combination of linear programming (LP) for the operation problem and genetic algorithm (GA) for the planning problem. Instead of such a multi-stage approach, this paper formulates the integrated planning and operation problem in terms of a single-stage, mixed-integer quadratic program (MIQP). The advantage of the MIQP formulation lies in the ability to utilize computationally efficient commercial optimization solvers, e.g., CPLEX and Gurobi, and also in the possibility of deploying decomposition techniques, e.g., Benders decomposition, for potential large-scale problems. To this end, linear thermal building and electric grid models are formulated to express the occupants comfort and the electric grid constraints.

In section 2, the required input data and workflow of the proposed framework is outlined. Section 3 presents the required pre-processing steps for the electric grid model. The linear electric grid and thermal building models are then formulated in section 4 and section 5. Section 6 discusses the setup of the numerical optimization problem. The test case is introduced in section 7 and the results and discussion follow in section 8. Lastly, concluding remarks are compiled in section 9.

Nomenclature

Let $\mathbb{R}$ be the domain of real numbers. Non-bold letters x, X denote scalars $\mathbb{R}^{1\times1}$, bold lowercase letters $\boldsymbol{x}$ denote vectors $\mathbb{R}^{n\times1}$ and bold uppercase letters $\boldsymbol{X}$ denote matrices $\mathbb{R}^{n\times m}$. The transpose of a vector or matrix is denoted by $()^\intercal$. Symbols for physical properties are aligned with ISO 80000 and units are based on the international system of units (SI). Prices and costs are in Singapore dollars (SGD) which is denoted by S$.

Sets and indices

$\mathcal{T}$	Set of time steps
$\mathcal{N}$	Set of grid nodes
$\mathcal{L}$	Set of lines
$\mathcal{K}$	Set of line types
$\mathcal{Z}_b$	Set of zones in building b
$\mathcal{B}$	Set of buildings in the district
$\mathcal{S}_z$	Set of surfaces adjacent to zone z
$\mathcal{W}_z$	Set of windows adjacent to zone z
$t \in \mathcal{T}$	Time step
$i \in \mathcal{N}$	Grid node
$k \in \mathcal{K}$	Line type
$(i,j) \in \mathcal{L}$	Grid line connecting node i and j
$(i,j),k$	Grid line of line type k connecting node i and j
$z \in \mathcal{Z}_b$	Zone
$b \in \mathcal{B}$	Building
$s \in \mathcal{S}_z$	Surface
$w \in \mathcal{W}_z$	Window
d	Direction / orientation of a surface

Electric-grid-model variables and parameters

$P^{dem}_{i,t}$	Active power demand at node i and time step t	[W]
$P^{sup}_{i,t}$	Active power supply at node i and time step t	[W]
$P_{(i,j),k,t}$	Active power through line $(i,j),k$ at time step t	[W]
$X_{(i,j),k}$	Reactance of line $(i,j),k$	[Ω]
$R_{(i,j),k}$	Resistance of line $(i,j),k$	[Ω]
$L_{(i,j)}$	Length of line (i,j)	[m]
$\alpha_{(i,j),k}$	Integer variable representing whether line $(i,j),k$ is built $\alpha_{(i,j),k}=1$ or not $\alpha_{(i,j),k}=0$	[-]
$\omega_{(i,j),k,t}$	Auxiliary variable with the unit of power	[W]
P^{aux}	Auxiliary constant with the unit of power	[W]
θ_i	Voltage angle at node i	[rad]
$P^{sub,max}$	Maximum loading of the substation	[V A]
$p^{sub,max}$	Max. desired relative loading of substation transf.	[-]

P_b^{max}	Maximum loading of building b	[V A]
$P_{z,t}^{base,el}$	Fixed base electric consumption of zone z	[W]
$p^{bld,max}$	Max. desired relative loading of building transf.	[-]
I_k^{max}	Maximum current of line type k	[A]
V^{base}	Voltage level of the distribution grid	[V]
N^{bld}	Number of building nodes	[-]
N^{sub}	Number of substation nodes	[-]

Thermal-grid-model variables and parameters

T_z	Zone air temperature at zone z	[°C]
T_z^{min}	Minimum air temperature at zone z	[°C]
T_z^{max}	Maximum air temperature at zone z	[°C]
C_z^{th}	Thermal heat capacity of zone z	[J/(m^3 K)]
$\dot{Q}_{s,z}^{cnv,int}$	Convective heat transfer from surfaces s towards zone z	[W]
$\dot{Q}_z^{inf}$	Heat transfer to zone z due to infiltration	[W]
$\dot{Q}_z^{occ}$	Heat transfer to zone z due to occupancy gains	[W]
$\dot{Q}_z^{hvac,heat}$	Heat transfer to zone z from the HVAC system for heating	[W]
$\dot{Q}_z^{hvac,cool}$	Heat transfer to zone z from the HVAC system for cooling	[W]
$\dot{Q}_s^{cnv,ext}$	Conv. heat transfer from the exterior to surface s	[W]
$\dot{Q}_s^{irr,ext}$	Incident irradiation onto surface s	[W]
$\dot{Q}_s^{ems,sky}$	Emitted radiation from surface s to the sky	[W]
$\dot{Q}_s^{ems,gnd}$	Emitted radiation from surface s to the ground	[W]
$\dot{Q}_s^{ext,int}$	Conductive heat transfer from the exterior to the interior side of surface s	[W]
$\dot{Q}_{s,z}^{cnv,int}$	Convective heat transfer from surface s to zone z	[W]
$\dot{Q}_s^{irr,int}$	Incident irradiation reaching surface s through exterior windows adjacent to the same zone z	[W]
A_s	Surface area of surface s	[m^2]
h^{ext}	Exterior conv. heat transfer coefficient	[W/(m^2 K)]
T^{amb}	Ambient temperature	[°C]
$T_s^{sur,ext}$	Exterior surface temperature of surface s	[°C]
α_s	Irradiation absorption coefficient of surface s	[-]
h_s^{sky}	Sky emission heat transfer coefficient	[W/(m^2 K)]
σ	Stefan-Boltzmann constant	[W/(m^2 K^4)]
ε_s	Emission coefficient of surface s	[-]
F_d^{sky}	View factor of direction d towards the sky	[-]
$T_s^{sur,ext,lin}$	Linearization constant for $T_s^{sur,ext}$	[K]
$T^{sky,lin}$	Linearization constant for T^{sky}	[K]
h_s^{gnd}	Ground emission heat transfer coeff.	[W/(m^2 K)]
F_d^{gnd}	View factor of direction d towards the ground	[-]
$T^{amb,lin}$	Linearization constant for T^{amb}	[K]
h_d^{int}	Interior conv. heat transfer coefficient	[W/(m^2 K)]
$\dot{q}_z^{irr,int}$	Interior irradiation at zone z	[W/m^2]
τ_w	Transmission coefficient of the window w	[-]
$h_s^{ext,int}$	Conductive heat transfer coeff.	[W/(m^2 K)]
V_z	Volume of zone z	[m^3]
$C^{th,air}$	Heat capacity of air	[J/(m^3 K)]
n_z^{inf}	Infiltration rate	[1/h]
$\dot{q}_z^{occ}$	Specific thermal gain due to occupancy	[W/m^2]
$\eta_b^{hvac,heat}$	Eff. factor for heating through the HVAC system	[-]
$\eta_b^{hvac,cool}$	Eff. factor for cooling through the HVAC system	[-]
$P_z^{hvac,heat}$	Elc. demand of the HVAC system for heating	[W]
$P_z^{hvac,cool}$	Elc. demand of the HVAC system for cooling	[W]

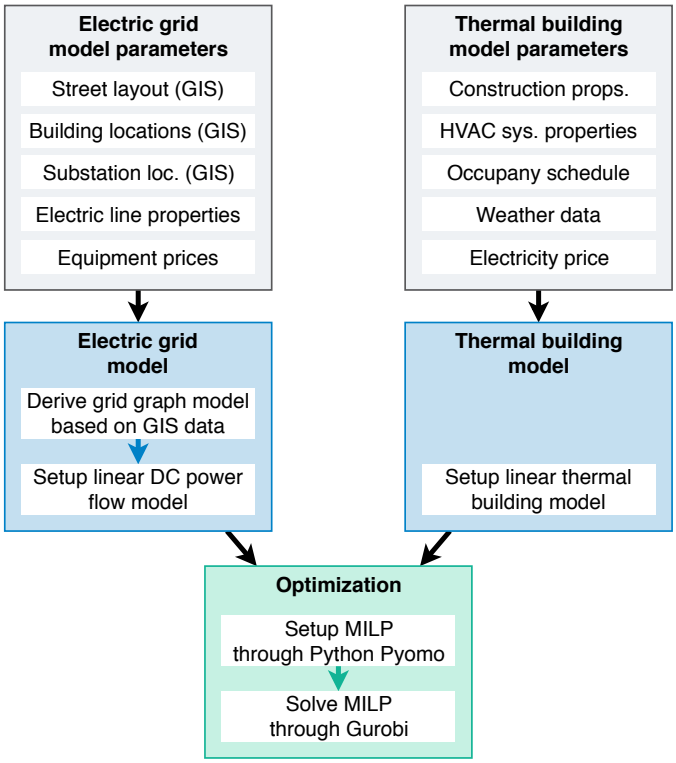

Figure 1: Workflow for the optimal planning and operation framework.

$\boldsymbol{x}$	State vector	[-]
$\boldsymbol{u}$	Input vector	[-]
$\boldsymbol{v}$	Disturbance vector	[-]
$\boldsymbol{A}$	State matrix	[-]
$\boldsymbol{B}_u$	Input matrix	[-]
$\boldsymbol{B}_v$	Disturbance matrix	[-]

Cost variables and parameters

$J^{inv,lin}$	Investment cost for electric grid lines	[S$]
$J^{inv,sub}$	Investment cost for substations	[S$]
$J^{inv,bld}$	Investment cost for building level transformers	[S$]
$J^{op,loss}$	Operation cost for electric line losses transformers [S$]	
$J^{op,bld}$	Operation cost for all buildings	[S$]
f^{ann}	Annuity factor for electric grid investments	[-]
f^{intr}	Interest rate	[-]
f^{mnt}	Maintenance cost factor	[-]
n^{life}	No. of years' expec. lifetime of elec. grid equip.	[-]
k_k^{inv}	Specific investment cost of line type k	[S$/m]
$c^{inv,sub}$	Specific investment cost of the substation	[S$/VA]
$c^{inv,sub}$	Specific inv. cost of the building transf.	[S$/VA]
c^{elc}	Price of electricity	[S$/Wh]

2. Methodology

2.1. Workflow and required inputs

Figure 1 depicts the workflow for the proposed optimal planning and operation framework. The main steps are 1) the setup of the electric grid model, 2) the setup of the thermal building

model and 3) the setup and solving of the numerical optimization problem.

The input data required for the proposed planning and operation framework consists of electric grid model data and building model data. The electric grid data consists of the street layout, building and substation locations in terms of geographic information system (GIS) data as well as the electric lines' conductor properties and the acquisition and installation costs of the electric grid equipment. Note that while this paper only considers the costs for lines, substations and building level transformers, further costs for secondary equipment such as breakers and sensors can easily be considered through extensions of the algorithm. The thermal building data consists of construction properties, i.e., geometric and technical information about the building structure, including its intended occupancy structure, along with HVAC system properties, occupancy schedule, weather data and the electricity price. Note that the disturbances to the building operation such as weather and occupancy schedules are projected for the planning time horizon based on test reference year data for the weather and reference occupancy schedules are based on international norms. In terms of weather data, the test reference year is considered a robust estimate as it contains historical worst-case scenarios for both hot and cold periods. In terms of the occupancy schedule, the solution can be made robust by considering the worst-case scenario for any occupancy schedule, e.g., by defining a higher-than-expected occupancy density.

In setting up the electric grid model, the GIS data is first pre-processed to derive a grid graph model in terms of nodes, i.e., substation and building connection points, and lines, i.e., possible interconnections and line lengths between the nodes. Based on this information, a linear DC power flow model for the electric grid is formulated. Similarly, the linear thermal building model is generated based on the given construction properties and HVAC system properties for the building. Further data items, e.g., the electric grid equipment costs, occupancy schedule, weather data and electricity prices are passed along with the linear models for the setup of the optimization problem.

2.2. Optimization problem and interpretation

The planning and operation problem is formulated as a mixed-integer quadratic program (MIQP) in a single-stage optimization problem. The objective is to minimize the investment cost for the electric grid along with the operating cost for electric line losses and the operating cost for all buildings. The decision variables are the electric grid topology, i.e., the decision to build line interconnections, and the dispatch schedule for building HVAC systems. The thermal-comfort constraints and electric-line loading limits form the constraints of the MIQP. The linear thermal building model expresses the thermal-comfort constraints as a function of the scheduled electric load, whereas the linear power flow model translates the load schedule into the electric line loading. Note that the operating cost for electric line losses is the only quadratic term of the problem, while all other cost terms and constraints are linear or mixed-integer linear. The MIQP can be solved efficiently with common commercial solvers, e.g., Gurobi, CPLEX and MOSEK.

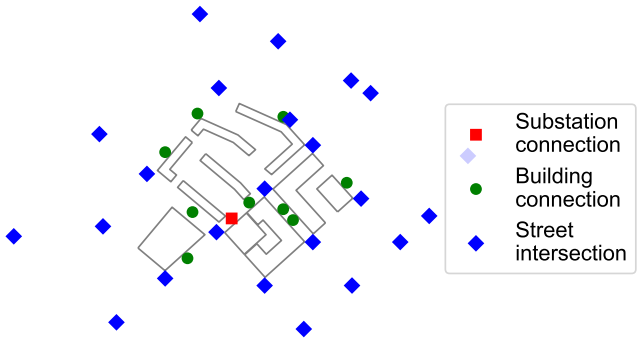

Figure 2: GIS data contained in the test case input data.

The planning and operation optimization problem can be interpreted as the combined social welfare maximization problem of all stakeholders of the districts' energy system. The problem is formulated in a centralized fashion to decrease the computational effort, although this formulation requires a level of oversight which is only realistic at the planning stage. In particular, the problem formulation suggests that the electric-grid operator is aware of each buildings' operational constraints and can directly control the HVAC dispatch schedule of each building such that electric-grid constraints are respected.

In the operation phase, i.e., once the electric grid and buildings have been installed, there exists a need to separate the concerns between the electric grid operator and the building operators. To this end, a local electricity market framework can be implemented which enables electric grid operators to incentivize the building operators to reschedule loads when electric grid constraints would be violated. Such frameworks have been suggested for the electric distribution grid in [14] based on a subgradient algorithm where the electric grid operator iteratively adjusts nodal electricity prices based on the projected demand schedules of the building operators, and in [17] where the building operators are submitting demand bids into a local peer-to-peer market which also applies a network usage charge. This paper does not model the interaction of electric grid operators and building operators in the operation phase, but assumes that such a framework will exist to ensure that the electric grid constraints can be maintained.

3. Electric grid pre-processing

The test case input data comprises the GIS data of the street network, substation location and the geometrical building shapes as depicted in fig. 2. This data is pre-processed to derive the nodes and all possible lines of the electric grid. The possible lines consist of all interconnections between all the nodes in the grid as depicted in (fig. 3). This accounts for the fact that distribution-grid line intersections only occur at grid nodes, i.e., buildings and substations, and not for example at street intersections [18]. Possible line paths are routed along the street network, as modern distribution grid lines are routed underground

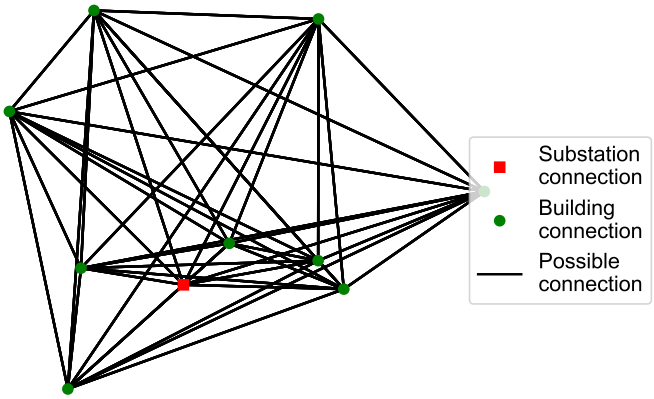

Figure 3: Potential electric grid inter-connections for the test case.

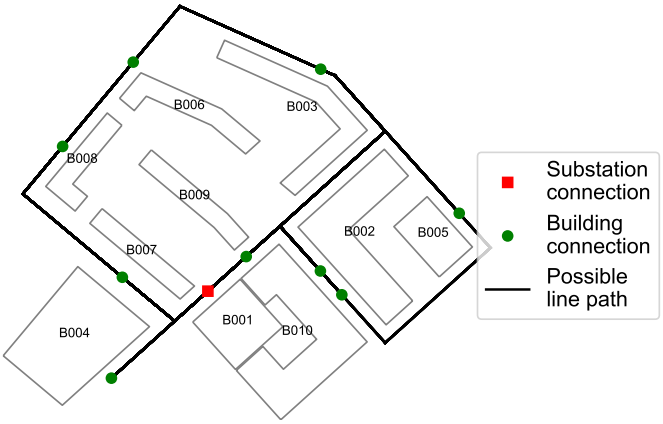

Figure 4: Potential electric grid line paths for the test case.

below streets. The path for each line is derived as the shortest path between the two nodes along the street network (fig. 4). Therefore, the building nodes, i.e., the points where the building transformers are connected to the electric distribution grid, are positioned along the streets. The locations of the building nodes (fig. 4) are found by seeking the shortest path from the centroid of the area of each building towards any nearby street.

4. Electric grid model

A DC power flow model is considered for the combined planning and operation problem, similarly to [13]. The presented formulation assumes that 1) all electric loads are connected in a three-phase-balanced manner and 2) all lines consist of three symmetric phases. An AC power flow model as in [18] can in principle be considered as well, but was avoided in this work to maintain a moderate number of decision variables and a better computational efficiency. However, the chosen DC power flow model necessitates validating the solution of the planning and operation problem with a high-fidelity power solver, to ensure the feasibility of the power flow before the deployment of the electric grid.

As a starting point, the power balance of the electric grid is expressed as:

$$P^{sup}_{i,t} - P^{dem}_{i,t} = \sum_{\substack{(i,j)\in\mathcal{L} \\ k\in\mathcal{K}}} P_{(i,j),k,t} \tag{1}$$

where $P^{dem}_{i,t}$ and $P^{sup}_{i,t}$ are the active power demand and the active power supply at each grid node $i \in \mathcal{N}$ and time step $t \in \mathcal{T}$, whereas $P_{(i,j),k,t}$ is the active power flowing in grid line $(i,j),k$ connecting the nodes i and j of line type $k \in \mathcal{K}$. The set $\mathcal{L}$ contains all grid lines (i,j), set $\mathcal{K}$ contains all line types, set $\mathcal{N}$ contains all grid nodes and set $\mathcal{T}$ contains all time steps.

The power flow $P_{(i,j),k,t}$ across each line $(i,j),k$ at time step t is expressed as:

$$\frac{P_{(i,j),k,t}}{3} = V^2_{base}\frac{\theta_{i,t} - \theta_{j,t}}{X_{(i,j),k}} + \omega_{(i,j),k,t} \tag{2}$$

where θ_i, θ_j are the voltage angles of the nodes i, j and $X_{(i,j),k}$ is the reactance of the line $(i,j),k$. The factor $\frac{1}{3}$ takes into account that each line consists of three phase conductors and $X_{(i,j),k}$ is defined for a single conductor. The symbol $\alpha_{(i,j),k}$ is an integer variable $\alpha_{(i,j),k} \in 0,1$ which describes the decision to build line $(i,j),k$, i.e., the line only exists when $\alpha_{(i,j),k} = 1$. The auxiliary variable $\omega_{(i,j),k,t}$ ensures that $P_{(i,j),k,t}$ can take the value of zero, in case the decision variable $\alpha_{(i,j),k}$ is assigned to the value of zero and no line is built between node i and j.

The auxiliary variable $\omega_{(i,j),k,t}$ is expressed as:

$$|\omega_{(i,j),k,t}| \leq (1 - \alpha_{(i,j),k})P^{aux} \tag{3}$$

where $P^{aux} \gg P_{(i,j),k,t}$ is an auxiliary constant, i.e., P^{aux} can be any very large number.

5. Thermal building model

The thermal loads of a building can be shifted by leveraging its thermal inertia. This allows the electric load of the HVAC system to be shifted, by pre-cooling or pre-heating a building while maintaining an admissible interval of thermal-comfort constraints. In this work, the thermal comfort is expressed in terms of the indoor air temperature. Hence, the thermal building model expresses the relationship between the indoor air temperature, the electric load of the HVAC system, the local weather conditions and the building occupancy.

In the considered test case, each building comprises one zone per occupancy type, where the indoor air temperature, i.e., the zone temperature, within each zone is uniformly distributed and there is no heat transfer between zones of differing occupancy types.

As a starting point, the differential equation of the zone temperature T_z of zone z is expressed as:

$$\frac{dT_z}{dt} = \frac{1}{C_{th,z}}\cdot\Bigg(\Bigg(\sum_{s\in\mathcal{S}_z}\dot{Q}^{cnv,int}_{s,z}\Bigg) + \dot{Q}^{inf}_z + \dot{Q}^{occ}_z + \dot{Q}^{hvac,heat}_z + \dot{Q}^{hvac,cool}_z\Bigg) \tag{4}$$

where C_z^{th} is the thermal heat capacity of zone $z \in \mathcal{Z}_b$, which is obtained according to ISO 13790. The symbol $\mathcal{Z}_b$ is the set of all zones z in building $b \in \mathcal{B}$ and $\mathcal{B}$ is the set of all buildings b. The heat transfer towards zone z is composed of the convective heat transfer $\dot{Q}_{s,z}^{cnv,int}$ from surfaces $s \in \mathcal{S}_z$ towards zone z, heat transfer towards zone z due to infiltration $\dot{Q}_z^{inf}$, heat transfer towards zone z due to occupancy gains $\dot{Q}_z^{occ}$ and heat transfer towards zone z from the HVAC system for heating $\dot{Q}_z^{hvac,heat}$ as well as cooling $\dot{Q}_z^{hvac,cool}$, where $\mathcal{S}_z$ is the set of all surfaces adjacent to zone z.

The ground heat transfer is neglected in this work, because all buildings in the considered test case have a low footprint-to-volume ratio. All other heat transfer models are formulated in the following subsections.

5.1. Exterior surfaces

Exterior surfaces are modelled as a thermal resistance between the exterior and zone z. Each surface s is adjacent to exactly one zone z. The heat transfer across exterior surface s is described by the balance equation for the exterior side:

$$\dot{Q}_s^{cnv,ext} + \dot{Q}_s^{irr,ext} - \dot{Q}_s^{ems,sky} - \dot{Q}_s^{ems,gnd} = \dot{Q}_s^{ext,int} \tag{5}$$

where $\dot{Q}_s^{cnv,ext}$ is the convective heat transfer from the exterior towards surface s, $\dot{Q}_s^{irr,ext}$ is the incident irradiation onto surface s, and $\dot{Q}_s^{ems,sky}$ and $\dot{Q}_s^{ems,gnd}$ are the emitted radiation from surface s towards the sky and the ground, respectively. The symbol $\dot{Q}_s^{ext,int}$ describes the heat transfer from the exterior towards the interior side of the surface.

The balance equation for the interior side of surface s is expressed as:

$$\dot{Q}_s^{ext,int} = \dot{Q}_{s,z}^{cnv,int} - \dot{Q}_s^{irr,int} \tag{6}$$

On the interior side, $\dot{Q}_{s,z}^{cnv,int}$ is the convective heat transfer from surface s towards zone z and $\dot{Q}_s^{irr,int}$ is the incident irradiation reaching surface s through exterior windows adjacent to the same zone z.

The exterior convective term $\dot{Q}_s^{cnv,ext}$ is expressed as:

$$\dot{Q}_s^{cnv,ext} = A_s h^{ext} \left(T^{amb} - T_s^{sur,ext} \right) \tag{7}$$

where A_s is the surface area of surface s and h^{ext} is the exterior heat transfer coefficient which is given according to ISO 6946 as $h^{ext} = \left(0.04\,\mathrm{m^2\,K/W}\right)^{-1}$. The symbol T^{amb} is the ambient temperature and $T_s^{sur,ext}$ is the exterior surface temperature of surface s.

The exterior irradiation term $\dot{Q}_s^{irr,ext}$ is expressed as:

$$\dot{Q}_s^{irr,ext} = A_s \alpha_s \dot{q}_d^{irr,ext}, \quad d = d(s) \tag{8}$$

where α_s is the absorption coefficient of surface s assuming a uniform absorption across the spectrum of the incident irradiation. The symbol $\dot{q}_d^{irr,ext}$ is the total incident irradiation onto a surface oriented towards direction $d \in \{N, E, S, W, H\}$, i.e., vertically facing North N, East E, South S, West W or horizontally facing upwards H, depending on the respective surface's orientation $d = d(s)$.

The exterior sky emission term $\dot{Q}_s^{ems,sky}$ describes the radiative heat loss through emission towards the sky. The term is expressed as:

$$\dot{Q}_s^{ems,sky} = A_s h_s^{sky} \left(T_s^{sur,ext} - T^{sky} \right) \tag{9}$$

In this linear approximation, the symbol h_s^{sky} is introduced as the sky heat transfer coefficient of surface s, whereas T^{sky} is the sky temperature. The sky heat transfer coefficient h_s^{sky} in turn is defined as:

$$h_s^{sky} = 4\sigma\varepsilon_s F_d^{sky} \left(\frac{T_s^{sur,ext,lin} + T^{sky,lin}}{2} \right)^3 \tag{10}$$

where σ, ε_s and F_d^{sky} are the Stefan-Boltzmann constant, the surface emission coefficient of surface s for long-wave radiations and the view factor of direction $d(s)$ towards the sky, respectively. The temperatures $T_s^{sur,ext,lin}$ and $T^{sky,lin}$ are linearization constants that are defined as the average values of $T_s^{sur,ext}$ and T^{sky}.

The exterior ground emission term $\dot{Q}_s^{ems,gnd}$ describes the radiative heat loss through emission towards the ground as well as the built environment. The term is expressed similarly to $\dot{Q}_s^{ems,sky}$ as:

$$\dot{Q}_s^{ems,gnd} = A_s h_s^{gnd} \left(T_s^{sur,ext} - T^{amb} \right) \tag{11}$$

where h_s^{gnd} is introduced as the ground heat transfer coefficient of surface s, whereas T^{amb} is the ambient temperature. The sky heat transfer coefficient h_s^{gnd} in turn is defined as:

$$h_s^{sky} = 4\sigma\varepsilon_s F_d^{gnd} \left(\frac{T_s^{sur,ext,lin} + T^{amb,lin}}{2} \right)^3 \tag{12}$$

where F_d^{gnd} is the view factor of direction $d(s)$ towards the ground. The temperatures $T_s^{sur,ext,lin}$ and $T^{amb,lin}$ are linearization constants that are defined as the average values of $T_s^{sur,ext}$ and T^{amb}.

The interior convective term $\dot{Q}_{s,z}^{cnv,int}$ is expressed as:

$$\dot{Q}_s^{cnv,int} = A_s h_d^{int} \left(T^z - T_s^{sur,int} \right) \tag{13}$$

where h_d^{int} and T^z are the interior heat transfer coefficient and the zone air temperature. The interior heat transfer coefficient h_d^{int} depends on the surface's direction $d(s)$. According to ISO 6946, the term is expressed as:

$$h_d^{int} = \begin{cases} \left(0.13\,\mathrm{m^2\,K/W}\right)^{-1} & \text{for } d \in \{N, E, S, W\} \\ \left(0.17\,\mathrm{m^2\,K/W}\right)^{-1} & \text{for } d = H \end{cases} \tag{14}$$

The interior irradiation term $\dot{Q}_s^{irr,int}$ is expressed as:

$$\dot{Q}_s^{irr,int} = A_s \alpha_s \dot{q}_z^{irr,int}, \quad d = d(s) \tag{15}$$

where $\dot{q}_z^{irr,int}$ is the interior irradiation incident to all surfaces of zone z. The interior radiation $\dot{q}_z^{irr,int}$ is in fact the irradiation which has entered zone z by passing through adjacent windows,

and is assumed to be uniformly distributed to all surfaces. This term is expressed as:

$$\dot{q}_z^{irr,int} = \frac{\sum_{w \in \mathcal{W}_z} A_w \tau_w \dot{q}_{d(w)}^{irr,ext}}{\sum_{s \in \mathcal{S}_z} A_s} \tag{16}$$

where τ_w is the transmission coefficient of the window w. The sets $\mathcal{W}_z$ and $\mathcal{S}_z$ contain all windows w and surfaces s that are adjacent to zone z.

Finally, the coupling term $\dot{Q}_s^{ext,int}$ is expressed as:

$$\dot{Q}_s^{ext,int} = A_s h_s^{ext,int} \left(T_s^{sur,ext} - T_s^{sur,int} \right) \tag{17}$$

where $h_s^{ext,int}$ is the heat transfer coefficient through surface s.

The complete convective heat transfer $\dot{Q}_s^{cnv,zone}$ from surface s towards zone z which is needed for eq. (4) can be obtained by solving the overdetermined equation system in eq. (5) to eq. (17). After eliminating the surface temperatures $T_s^{sur,ext}$ and $T_s^{sur,int}$, the heat transfer through surface s towards zone z can be expressed as:

$$\begin{aligned}
\dot{Q}_s^{cnv,zone} = & \\
& \left(\alpha_s \dot{q}_d^{irr,ext} + h^{cnv,ext} \left(T^{amb} - T_s \right) \right. \\
& \left. + h_s^{gnd} \left(T^{amb} - T_s \right) + h_s^{sky} \left(T^{sky} - T_s \right) \right) \\
& \cdot A_s \left(1 + \frac{h^{cnv,ext} + h_s^{gnd} + h_s^{sky}}{h_s^{cnv,int}} \right. \\
& \left. + \frac{h^{cnv,ext} + h_s^{gnd} + h_s^{sky}}{h_s^{cnd}} \right)^{-1} \\
& + \alpha_s \dot{q}_z^{irr,int} \\
& \cdot A_s \left(1 - \left(\frac{1}{h^{cnv,ext} + h_s^{gnd} + h_s^{sky}} \right. \right. \\
& \left. \left. + \frac{1}{h_s^{cnv,int}} + \frac{1}{h_s^{cnd}} \right)^{-1} \right)
\end{aligned} \tag{18}$$

5.2. Infiltration

The heat transfer towards zone z due to infiltration $\dot{Q}_z^{inf}$ is defined as:

$$\dot{Q}_z^{inf} = V_z C^{th,air} n_z^{inf} \left(T^{amb} - T_z \right) \tag{19}$$

where V_z is the volume of zone z, $C^{th,air}$ is the heat capacity of air and n_z^{inf} is the infiltration rate.

5.3. Occupancy gains

Assuming perfect knowledge of the building occupancy schedule, the heat transfer towards zone z due to occupancy gains $\dot{Q}_z^{occ}$, i.e., internal gains, is expressed as:

$$\dot{Q}_z^{occ} = A_z \dot{q}_z^{occ} \tag{20}$$

where A_z is the area of zone z and $\dot{q}_z^{occ}$ is the specific thermal gain due to occupancy.

5.4. HVAC system

The heat transfer towards zone z from the HVAC system for heating $\dot{Q}_z^{hvac,heat}$ and cooling $\dot{Q}_z^{hvac,cool}$ is expressed as:

$$\begin{aligned}
\dot{Q}_z^{hvac,heat} &= \eta_b^{hvac,heat} P_z^{hvac,heat} \\
\dot{Q}_z^{hvac,cool} &= -\eta_b^{hvac,cool} P_z^{hvac,cool}
\end{aligned} \tag{21}$$

where $\eta_b^{hvac,heat}$ and $\eta_b^{hvac,cool}$ is the efficiency factor for heating and cooling through the HVAC system of building b. Furthermore, $P_z^{hvac,heat}$ and $P_z^{hvac,cool}$ are the electric power consumption of the HVAC system associated with heating and cooling demand at zone z.

5.5. State space form

Finally, the thermal building model is transformed into state space form, because this allows for a more compact representation which is independent from changes in model configuration or size:

$$\dot{\boldsymbol{x}} = \boldsymbol{A}\boldsymbol{x} + \boldsymbol{B}_u \boldsymbol{u} + \boldsymbol{B}_v \boldsymbol{v} \tag{22}$$

where the vectors $\boldsymbol{x}$, $\boldsymbol{u}$ and $\boldsymbol{v}$ are the state, input and disturbance vectors. The matrices $\hat{\boldsymbol{A}}$, $\hat{\boldsymbol{B}}_u$ and $\hat{\boldsymbol{B}}_v$ are the state, input and disturbance matrices. Note that the state space model in eq. (22) is simply a representation of the differential equation for the zone temperature in eq. (4), where the model variables are arranged into the vectors as follows:

$$\begin{aligned}
\boldsymbol{x} &= \left[T_z \right]_{z \in \mathcal{Z}_b,\ b \in \mathcal{B}} \\
\boldsymbol{u} &= \left[\left[P_z^{hvac,heat} \right]_{z \in \mathcal{Z}_b,\ b \in \mathcal{B}}^{\mathsf{T}}, \left[P_z^{hvac,cool} \right]_{z \in \mathcal{Z}_b,\ b \in \mathcal{B}}^{\mathsf{T}} \right]^{\mathsf{T}} \\
\boldsymbol{v} &= \left[T^{amb}, T^{sky}, \left[\dot{q}_d^{irr,ext} \right]_{d \in \{N,E,S,W,H\}}^{\mathsf{T}} \right]^{\mathsf{T}}
\end{aligned} \tag{23}$$

The time-discrete form of the thermal building model which is required for the optimization problem is obtained by application of zero-order hold discretization, where $\hat{()}$ denotes the discretized matrices:

$$\boldsymbol{x}_{t+1} = \hat{\boldsymbol{A}} \boldsymbol{x}_t + \hat{\boldsymbol{B}}_u \boldsymbol{u}_t + \hat{\boldsymbol{B}}_v \boldsymbol{v}_t \quad \forall t \in \mathcal{T} \tag{24}$$

6. Optimization problem

The optimal planning and operation problem is expressed as an optimization problem for minimizing the investment cost for the electric grid, along with the operating cost for electric line losses and the operating cost for all buildings. The investment cost comprises the annualized investment costs for the electric grid lines and substations as well as annualized maintenance costs of the electric grid equipment. The operating cost of electric line losses takes into account the the electricity cost associated with such losses. The cost of operation for all buildings considers the annualized electricity cost for the HVAC system and the fixed base demand. The constraints of the optimization problem are the linear electric grid model, the linear thermal building model, electric grid constraints and thermal-comfort constraints.

6.1. Cost function

The total cost J is expressed as:

$$\min \quad J = J^{inv,lin} + J^{inv,sub} + J^{inv,bld} + J^{op,loss} + J^{op,bld} \tag{25}$$

where $J^{inv,lin}$, $J^{inv,sub}$ and $J^{inv,bld}$ are the annualized investment cost for all electric grid lines, substations and building level transformers. The symbols $J^{op,loss}$ and $J^{op,bld}$ describe the annualized operating cost of electric line losses and the operating cost for all buildings.

In the following, the annuity factor f^{ann} expresses the equivalent annual cost of the electric grid investments based on their net present value [19] and is defined as:

$$f^{ann} = \frac{\left(1 + f^{intr}\right)^{n^{life}} \cdot f^{intr}}{\left(1 + f^{intr}\right)^{n^{life}} - 1} \tag{26}$$

where f^{intr} is the interest rate and n^{life} is the expected lifetime of the electric grid equipment.

The annualized investment cost for the electric grid lines $J^{inv,lin}$ is expressed as:

$$J^{inv,lin} = \left(\sum_{\substack{(i,j)\in\mathcal{L} \\ k\in\mathcal{K}}} \alpha_{(i,j),k} L_{(i,j)} k_k^{inv} \right) f^{ann} (1 + f^{mnt}) \tag{27}$$

where $L_{(i,j)}$ is the length of line (i, j), k_k^{inv} is the specific cost of line type k and f^{ann} is its annuity factor. The symbol f^{mnt} is the maintenance cost factor.

The annualized investment cost for the substation $J^{inv,sub}$ are expressed as follows:

$$J^{inv,sub} = \frac{P^{sub,max}}{p^{sub,max}} c^{inv,sub} f^{ann} (1 + f^{mnt}) \tag{28}$$

where $P^{sub,max}$ is the maximum loading of the substation, $c^{inv,sub}$ is the specific investment cost and $p^{sub,max}$ is the maximum desired relative loading for the substation. The cost of losses in the transformers is not directly considered in this formulation. Instead, the maximum desired relative loading $p^{sub,max}$ is provided as a parameter to enable limiting the transformer load.

The annualized investment cost for the building transformers $J^{inv,bld}$ is expressed as:

$$J^{inv,bld} = \frac{P_b^{max}}{p^{bld,max}} c^{inv,bld} f^{ann} (1 + f^{mnt}) \tag{29}$$

where P_b^{max} is the maximum loading of each building, $c^{inv,sub}$ is the specific investment cost and $p^{bld,max}$ is the maximum desired relative loading for the building transformers.

The annualized operating cost for electric line losses $J^{op,loss}$ is calculated according to:

$$J^{op,loss} = \sum_{t\in\mathcal{T}} \sum_{\substack{(i,j)\in\mathcal{L} \\ k\in\mathcal{K}}} \left(\frac{P_{(i,j),k,t}}{\sqrt{3}\, V^{base}} \right)^2 \frac{R_{(i,j),k}}{3} c^{elc} \tag{30}$$

where $P_{(i,j),k,t}$ is the power flow across line $(i, j), k$, V^{base} is the voltage level of the distribution grid $R_{(i,j),k}$ is the resistance of the line and c^{elc} is the price of electricity. The factor $\frac{1}{3}$ takes into account that each line consists of three phase conductors and $R_{(i,j),k}$ is defined for a single conductor. Note that the optimization problem becomes a mixed-integer quadratic program (MIQP) due to the quadratic term of the decision variable $P_{(i,j),k,t}$, whereas all other objective and constraint terms are either linear or mixed-integer linear.

The operating cost J_b^{elc} for each building b is expressed as:

$$J^{op,bld} = \sum_{t\in\mathcal{T}} \sum_{\substack{z\in\mathcal{Z}_b \\ b\in\mathcal{B}}} \left(P_{z,t}^{hvac,el} + P_{z,t}^{base,el} \right) c^{elc} \tag{31}$$

where c_{elc} is the electricity price and $P_{z,t}^{base,el}$ is the fixed base electric consumption of each zone z, e.g., for lighting and appliances.

6.2. Electric grid constraints

The thermal limits of the electric grid equipment are defined as a function of the decision variables $\alpha_{(i,j),k}$, $P^{sub,max}$ and P_b^{max}:

$$\begin{aligned} \frac{|P_{(i,j),k,t}|}{3} &\le \alpha_{(i,j),k}\, I_k^{max} \sqrt{3}\, V^{base} && \forall (i,j) \in \mathcal{L},\ \forall k \in \mathcal{K},\ \forall t \in \mathcal{T} \\ P_t^{sub} &\le P^{sub,max} && \forall t \in \mathcal{T} \\ P_{b,t}^{hvac} &\le P_b^{max} && \forall b \in \mathcal{B},\ \forall t \in \mathcal{T} \end{aligned} \tag{32}$$

where I_k^{max} and V^{base} are the maximum allowable of line type k and the voltage level of the distribution grid. The factor $\frac{1}{3}$ considers that each line consists of three phase conductors and I_k^{max} is defined for a single conductor. Note that this also ensures that no power is flowing across lines $(i, j), k$ for which $\alpha_{(i,j),k}$ is zero.

Electric distribution grids are usually operated in radial structures. To respect this form of configuration, the number of lines is limited according to:

$$\sum_{\substack{(i,j)\in\mathcal{L} \\ k\in\mathcal{K}}} \alpha_{(i,j),k} = 2 \left(N^{bld} - N^{sub} \right) \tag{33}$$

where N^{bld} and N^{sub} are the number of building nodes and the number of substation nodes.

Lastly, connections between any two nodes (i, j) are limited to one line $(i, j), k$ according to:

$$\sum_{k\in\mathcal{K}} \alpha_{(i,j),k} \le 1 \quad \forall (i,j) \in \mathcal{L} \tag{34}$$

Note that isolated nodes are avoided implicitly by the electric grid model equations (eq. (1), eq. (2) and eq. (3)), i.e., electric demand at building nodes must be satisfied through at least one line's power flow, and power supply can only be obtained from the substation node. Therefore, no additional explicit constraint is added here.

6.3. Thermal comfort constraints

The thermal comfort constraint is formulated based on the proposed thermal building model as:

$$\left[T_z^{min}\right]_{z\in\mathcal{Z}_b,\ b\in\mathcal{B}} \leq \boldsymbol{x}_t \leq \left[T_z^{max}\right]_{z\in\mathcal{Z}_b,\ b\in\mathcal{B}} \quad \forall t \in \mathcal{T} \tag{35}$$

where T_z^{min} and T_z^{max} are the minimum and maximum permissible air temperature in zone z, whose values depend on the zone's occupancy type.

7. Test case

The test case is based on a real greenfield urban planning project which is embedded in the port area of Tanjong Pagar, Singapore. In the near future, the port will be restructured into a multipurpose area, consisting of commercial, residential and office buildings. The test case is illustrated in fig. 2 and covers an approximate area of 300 000 m^2. In the chosen scenario, 10 buildings are included.

7.1. Electric grid model parameters

The electric distribution grid in Singapore is operated at V^{base} = 22 kV. The possible electric grid line paths and interconnections are derived according to section 3 based on the GIS data of the test case. The data for electric grid line types in table 1 are derived from local market data based on the work of [18], which was cross-validated with reference values from [20] and [21]. The specific price for substations (66 kV / 22 kV) and building transformers (22 kV / 0.4 kV) is based on [20] and [21]. All the specific prices include the cost incurred by civil works, i.e., earthworks and installation. For the electricity price, the average of the Universal Singapore Energy Price (USEP) of 2017 is taken from [22]. These cost parameters are given in table 2.

Table 1: Electric line type data.

No.	Cross-section [mm^2]	Resistance [Ω/km]	Reactance [Ω/km]	Max. current [A]	Price [S$/m]
0	10	2.54	0.165	65	41.86
1	50	0.487	0.135	163	74.42
2	185	0.127	0.114	325	113.74

7.2. Thermal building model parameters

The geometric information of zones and surfaces, e.g., A_s, is derived from the GIS data of the test case. Based on the default Singapore database of CEA [23], the heat transfer coefficient $h_s^{ext,int}$, the absorption coefficient α_s, the emissivity ε_s of each surface s the transmissivity τ_w of each window w, the thermal capacity C_z^{th} according to ISO 13790 and the infiltration rate n_z^{inf} of each zone z are defined. Further, the HVAC system heating efficiency $\eta_b^{hvac,heat}$ and cooling efficiency $\eta_b^{hvac,cool}$ are calculated according to CEA, based on the building's system setup. The average annualized consumption of the buildings was cross-validated against historic values from Singapore's building and construction authority (BCA) [24].

Table 2: Electric grid planning parameters.

Parameter	Value
$c^{inv,sub}$	30 S$/kVA
$p^{sub,max}$	75 %
$c^{inv,bld}$	50 S$/kVA
$p^{bld,max}$	75 %
c^{elc}	80.9 S$/MWh
f^{intr}	5 %
n^{life}	40
f^{mnt}	0.04

Table 3: Thermal building model parameters.

Parameter	Value
F_d^{sky} $(\forall d \in \{N, E, S, W\})$	0.5
F_d^{gnd} $(\forall d \in \{N, E, S, W\})$	0.5
F_d^{sky} $(d = H)$	1
F_d^{gnd} $(d = H)$	0

Table 4: Thermal model linearization parameters.

Parameter	Value
$T_s^{sur,ext,lin}$	35 °C
$T^{sky,lin}$	17 °C
$T^{amb,lin}$	30 °C

7.3. Weather data

Weather data is obtained from the default Singapore database of CEA [23]. The data comprises data items for the ambient temperature T^{amb} and the global horizontal irradiation $\dot{q}_{glb,hor}^{irr,ext}$. The incident irradiation $\dot{q}_d^{irr,ext}$ for each surface direction d is calculated as a function of the global horizontal irradiation $\dot{Q}_{glb,hor}^{irr,ext}$ and the local time through the PVLIB toolbox [25]. The sky temperature T^{sky} is defined by an approximation for tropical climate as $T^{sky} = T^{amb} - 13$ K according to ISO 52016-1.

7.4. Occupancy scenarios

The occupancy schedule and the fixed base electric load schedule $P_{z,t}^{base,el}$ are defined according to the occupancy type databases of CEA [23]. Seven occupancy scenarios are defined for the district, to study the impact of different occupancy types on DSF and the outcome of the planning and operation problem. In these scenarios, all the buildings are assigned the share of occupancy types as given in table 5.

Table 5: Building occupancy shares for each occupancy scenario.

Occupancy scenario	Office	Retail	Residential
Mixed	33.33 %	33.33 %	33.33 %
Off.	100 %	0 %	0 %
Ret.	0 %	100 %	0 %
Res.	0 %	0 %	100 %
Off.-Ret.	50 %	50 %	0 %
Off.-Res.	50 %	0 %	50 %
Ret.-Res.	0 %	50 %	50 %

7.5. Fixed and flexible-load operation

Fixed and flexible-load operation scenarios are considered to evaluate the effectiveness of the integrated planning and operation approach. The fixed operation scenario refers to the status quo, where the building HVAC systems are operated such that the zone air temperature T_z follows a fixed set temperature T^{set}. In the flexible operation scenario, the zone air temperature T_z is constrained to stay within the thermal comfort limits T^{min} and T^{max}. The temperatures T^{set}, T^{min} and T^{max} are defined depending on the occupancy scenario according to the occupancy database of CEA [23]. Set temperature and thermal comfort limits are only enforced during operation hours, depending on the occupancy type. Note that for this Singapore-based test case, the set temperature is set equal to the maximum temperature limit $T^{set} = T^{max}$.

8. Results and discussion

Table 6: Annualized costs for the mixed-occupancy scen. and fixed load.

Cost type	Value [S$]	Share
Investment cost for lines	9,228	0.15 %
Investment cost for substation	60,153	0.95 %
Investment cost building transformers	100,255	1.58 %
Operation cost for line losses	3145	0.05 %
Operation cost for buildings	6,169,682	97.27 %
Total	6,342,463	100.00%

Table 6 documents the categorized cost for the mixed occupancy scenario with fixed-load operation. In this scenario, the operating cost for buildings makes up the majority, i.e., approx. 97 % of the annualized cost. Among the investment cost, the substation and building level transformers amount for the majority of the cost, i.e., approx. 94 % of the investment cost. The operating cost for electric line losses makes up only 0.05 % of the total cost, but is in the same order of magnitude as the electric line investment cost. In the following, all investment costs and the operating cost for electric line losses are combined into the total investment cost.

Figure 5 depicts the peak loads by occupancy scenario with fixed-load operation for each building. In fact, for each occupancy scenario, an identical peak load in W/m^2 is observed. This is due to the occupancy scenarios defining all buildings in the district to have identical properties except for their geometrical dimensions. Among all occupancy scenarios, the residential scenario has the lowest peak demand while the retail scenario has highest peak demand. This results from a relatively low occupancy density in residential buildings, whereas retail buildings, e.g., shopping malls, have a much higher occupancy density and therefore experience higher internal gains, i.e., thermal heat gains due to occupants and appliances, which necessitates more cooling to respect the thermal-comfort constraints.

The electric load schedule for each occupancy scenario is shown in fig. 6 for a weekday. For most occupancy scenarios, the peak demand is observed during the middle of the day, but only the residential occupancy scenario reaches its peak demand during the morning and early evening, which reflects the daily occupancy and appliance schedule of the respective occupancy scenarios. Note that the sum of fixed base electric demand $P^{base,el}$ and the electric demand of the HVAC system $P^{hvac,el}$ is shown. Hence, even for office buildings, the electricity demand is greater than zero during the night hours. The peak seen during early-morning hours for some occupancy scenarios can be explained by the requirement to cool down the building after it had heated up overnight.

Table 7: Categorized costs by occupancy scenario with fixed-load operation.

Occupancy scen.	Operation cost for build. [S$]	Investment cost [S$]	Total cost [S$]
Mixed	6,169,682	172,781	6,342,463
Off.	5,035,806	160,543	5,196,349
Ret.	9,000,195	266,176	9,266,371
Res.	2,652,693	75,075	2,727,768
Off.-Ret.	7,022,348	208,995	7,231,343
Off.-Res.	4,201,641	119,602	4,321,243
Ret.-Res.	6,433,439	178,473	6,611,912

Table 7 and fig. 7 show the categorized cost by occupancy scenario at fixed-load operation, whereas table 8 documents the same for flexible-load operation. The operating cost for buildings scales proportionally to the electricity demand and the investment cost proportional to the peak load. Because the electricity demand is largely proportional to the peak load across all occupancy scenarios, the total cost also scales proportionally to the peak loads.

Table 9 presents the cost difference by occupancy scenario under flexible-load operation, relative (table 7) to fixed-load operation (table 8). Across all occupancy scenarios, a slight

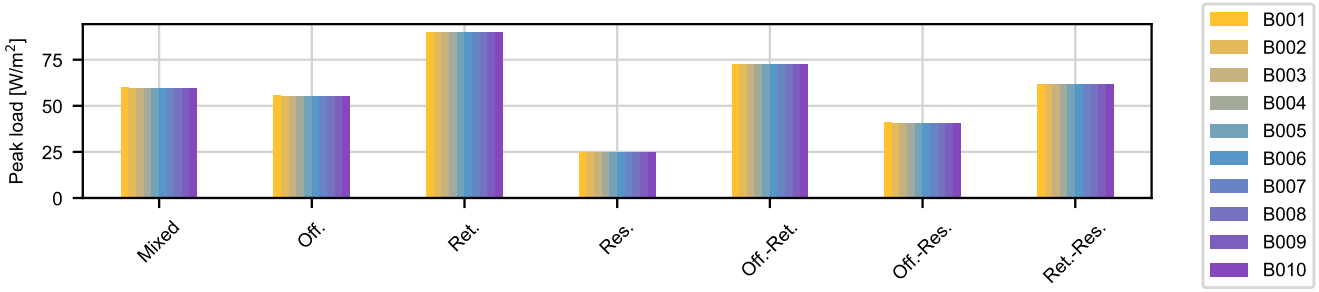

Figure 5: Building peak loads by occupancy scenario with fixed-load operation.

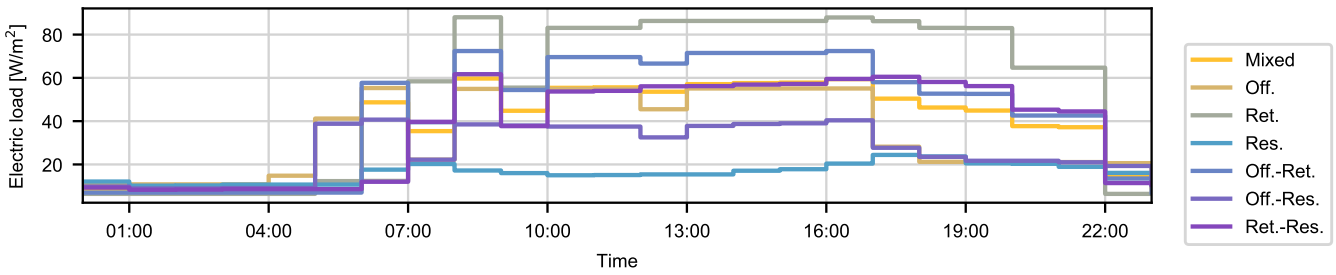

Figure 6: Electric load schedule by occupancy scenario with fixed-load operation.

Table 8: Categorized costs by occupancy scenario with flexible-load operation.

Occupancy scen.	**Operation cost for build.** [S$]	**Investment cost** [S$]	**Total cost** [S$]
Mixed	6,186,850	131,699	6,318,549
Off.	5,045,253	112,942	5,158,195
Ret.	9,035,032	175,144	9,210,176
Res.	2,655,810	58,193	2,714,003
Off.-Ret.	7,039,802	133,121	7,172,923
Off.-Res.	4,218,712	86,582	4,305,294
Ret.-Res.	6,454,145	141,472	6,595,617

Table 9: Cost difference by occupancy scenario.

Occupancy scen.	**Operation cost for build.**	**Investment cost**	**Total cost**
Mixed	+ 0.28 %	- 23.78 %	- 0.38 %
Off.	+ 0.19 %	- 29.65 %	- 0.73 %
Ret.	+ 0.39 %	- 34.20 %	- 0.61 %
Res.	+ 0.12 %	- 22.49 %	- 0.50 %
Off.-Ret.	+ 0.25 %	- 36.30 %	- 0.81 %
Off.-Res.	+ 0.41 %	- 27.61 %	- 0.37 %
Ret.-Res.	+ 0.32 %	- 20.73 %	- 0.25 %

increase in operating cost for buildings of up to 0.41 % is observed, along with a decrease in investment cost of up to 36.3 %, resulting in a total cost reduction of up to 0.81 %. The increase in operating cost for buildings results from an increase in thermal losses in the building when loads are shifted to a different time period, e.g., pre-cooling the building results in additional thermal losses across the buildings' surfaces during the pre-cooling period. However, even with this slight increase, the total annualized cost could be reduced for all occupancy scenarios as the reduction investment cost is more significant.

Table 10 presents the peak load and investment cost reduction by occupancy scenario with flexible-load operation relative to fixed-load operation. The results indicate that the investment cost reduction is proportional to the peak load reduction, which can be expected due to the investment cost consisting largely of substation and building transformer costs which are modelled as a function of the peak load according to eq. (28) and eq. (29).

Figure 8 and fig. 9 show the electric load schedule for the mixed office-retail occupancy scenario and the residential occupancy scenario, at both fixed and flexible-load operation. These occupancy scenarios are chosen because in table 10 the mixed office-retail occupancy scenario allows for the biggest relative cost reduction, whereas the residential occupancy scenario shows the smallest relative cost reduction. Comparing between the flexible and fixed-load operation for the office-retail scenario, the peak load reduction is largely due to pre-cooling the building in the early morning. In contrast, there is almost no pre-cooling in the residential scenario. The main reasons for the different behavior are 1) the different pattern of the peak loads and 2) the different overall level of the demand. Firstly, the peak load in the residential occupancy scenario occurs in the early evening, whereas it occurs in the middle of the day in the office-retail occupancy scenario. Hence, the pre-cooled

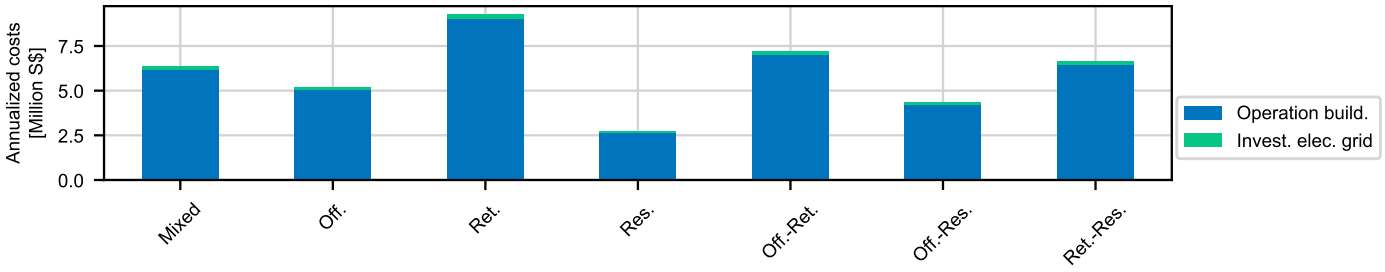

Figure 7: Categorized cost by occupancy scenario with fixed-load operation.

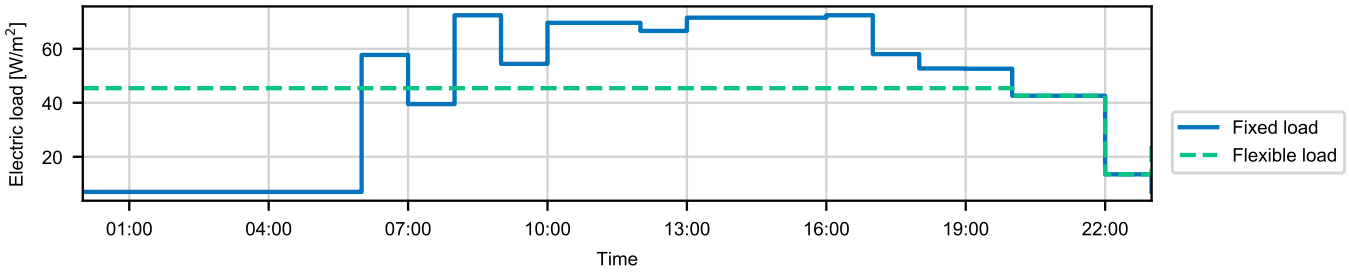

Figure 8: Electric load schedule for the mixed office-retail occupancy scenario.

Table 10: Peak load and investment cost reduction by occupancy scenario.

Occupancy scen.	**Absolute peak load change** [W/m^2]	**Relative peak load change**	**Investment cost change**
Mixed	- 14.74	- 24.73 %	- 23.78 %
Off.	- 16.91	- 30.63 %	- 29.65 %
Ret.	- 29.30	- 32.60 %	- 34.20 %
Res.	- 6.13	- 24.78 %	- 22.49 %
Off.-Ret.	- 26.99	- 37.28 %	- 36.30 %
Off.-Res.	- 11.73	- 28.93 %	- 27.61 %
Ret.-Res.	- 13.83	- 22.41 %	- 20.73 %

state would need to be maintained longer for the residential occupancy scenario, which would cause more significant thermal losses throughout the day. Secondly, in the residential occupancy scenario the peak loads under fixed-load operation are already relatively low, such that the buildings' demand can be satisfied largely with electric grid lines of type 0, and investment cost reduction would only be possible for substation and building transformer investments. Therefore, there is less incentive for peak load reduction in the residential scenario compared to the office-retail scenario.

Figure 10 and fig. 11 depict the electric grid layout for the retail occupancy scenario under fixed-load and flexible-load operation. Comparing flexible and fixed-load operation, the flexible-load operation permits the use of smaller line types due to the reduced peak loads.

9. Conclusions

This work presented a methodology for the planning of electric grids, with consideration for demand side flexibility of air-conditioned buildings. The integrated planning and operation problem was formulated as a mixed-integer quadratic program based on linear models for electric power flow and the thermal building dynamics. For a test case based in Singapore, the proposed methodology allows reductions of up to 36.3 % in investment costs, and of up to 0.81 % in total annualized cost. However, due to additional thermal losses caused by the shifting of electric loads, the annualized operating cost for buildings increased by up to 0.4 %.

The results of the test case offer insights to three groups of stakeholders in the district energy system. First, for governmental urban planning authorities, the results prove that demand side flexibility can readily improve the overall social welfare, since the total costs for planning and operation are effectively reduced with the presented methodology. Second, the urban developers and utility companies may note that there is significant potential for investment cost reduction through peak shaving with demand side flexibility, even though no additional energy storage deployment, i.e., thermal or battery storage at the building level, was considered in the presented test case. Third, for building operators who carry out operation and maintenance, the results indicate that there may be a trend towards dynamic electricity tariffs to enable demand side flexibility. The building operators should adapt their control capabilities, e.g., towards model predictive control, to be able to avoid the high peak prices. Additionally, the results also point towards closer collaboration between urban planners and building operators at

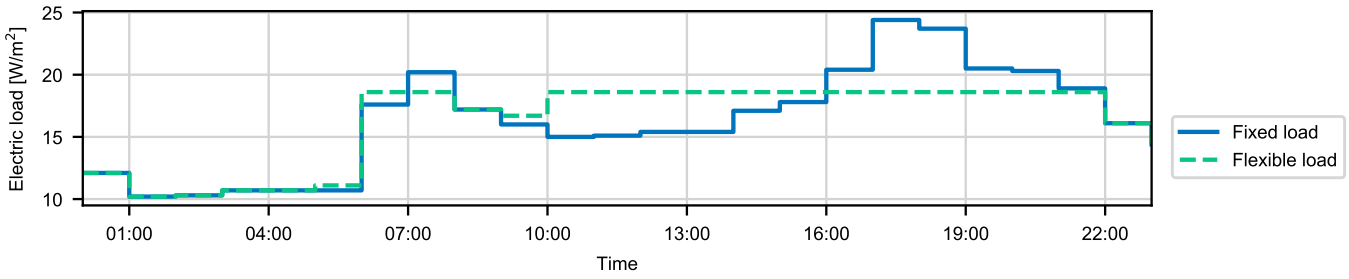

Figure 9: Electric load schedule for the residential occupancy scenario.

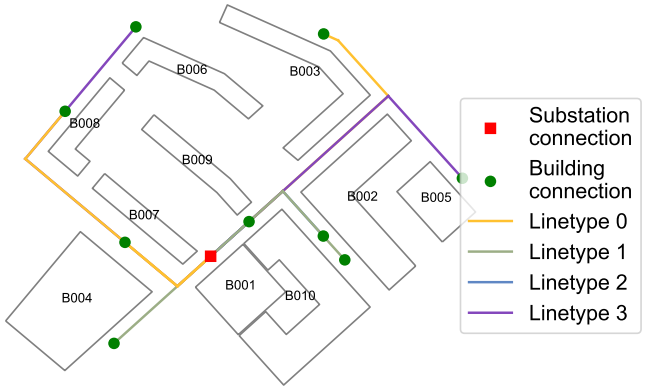

Figure 10: Electric grid layout for the retail occupancy scen. and fixed load.

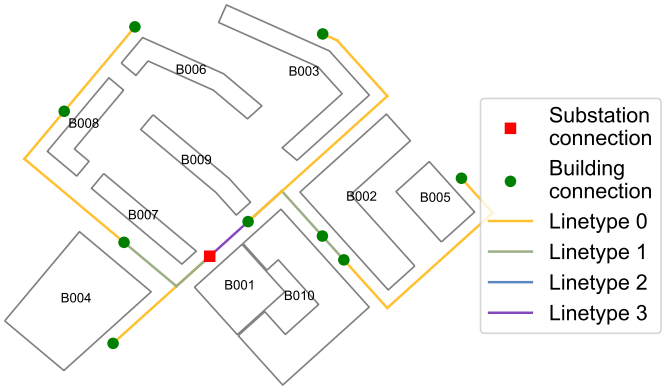

Figure 11: Electric grid layout for the retail occupancy scen. and flexible load.

the planning phase, such that appropriate demand side flexibility potential is leveraged for cost reduction.

The mixed office-retail occupancy scenario demonstrated the largest total cost reduction along with a high peak-shaving ability. In fact, demand side flexibility is also easier to achieve in the heating ventilation and air-conditioning system of such buildings, due to the existing centralized control architecture through a building management system and the highly predictable occupancy schedule. This highlights the need to tap into office and retail buildings as a prime resource for demand side flexibility.

The investment cost of the electric lines plays a minor role, i.e., approx. 3 %, in the investment decision of the presented test case. If this result can be validated for a larger test case with more buildings and a more complex street network, then the planning of the electric grid layout may in fact be performed downstream of the planning for the substation and building transformers. Such a hierarchical approach could lead to reduced computation time as the mixed-integer problem, i.e., the electric grid planning, can then be separated from the large-scale linear problem, i.e., optimal scheduling of flexible loads.

The algorithm has been integrated as a module in the city energy analyst [23] and as such is available online and open source. Future work will focus on utilizing higher-fidelity electric grid models, addressing uncertainty in weather and occupancy estimates, applying the algorithm to a larger test case and on taking a wider range of flexibility resources into account, e.g., battery and thermal energy storage systems.

Acknowledgment

This work was financially supported by the Singapore National Research Foundation under its Campus for Research Excellence And Technological Enterprise (CREATE) programme through the Intra-CREATE Seed Collaboration Grant project "Connecting District Energy and Power Systems for Future Singaporean New Towns" (NRF2016-ITS001-027).

References

[1] W. H. Kersting, Distribution System Modeling and Analysis, CRC Press, 2001.

[2] S. Hanif, C. Gruentgens, T. Massier, T. Hamacher, T. Reindl, Cost-optimal operation for a flexible building with local PV in a Singaporean environment, in: IEEE PES Innov. Smart Grid Technol. Conf., IEEE, 2016. doi:10.1109/ISGT.2016.7781232.

[3] R. Atia, N. Yamada, Sizing and Analysis of Renewable Energy and Battery Systems in Residential Microgrids, IEEE Trans. Smart Grid 7 (3) (2016) 1204–1213. doi:10.1109/TSG.2016.2519541.

[4] O. Sundstrom, C. Binding, Flexible Charging Optimization for Electric Vehicles Considering Distribution Grid Constraints, IEEE Trans. Smart Grid 3 (1) (2012) 26–37. doi:10.1109/TSG.2011.2168431.

[5] E. Vrettos, E. C. Kara, J. MacDonald, G. Andersson, D. S. Callaway, Experimental demonstration of frequency regulation by commercial buildings Part I: Modeling and hierarchical control design, IEEE Trans. Smart Griddoi:10.1109/TSG.2016.2628897.

[6] K. Chua, S. Chou, W. Yang, J. Yan, Achieving better energy-efficient air conditioning A review of technologies and strategies, Appl. Energy 104 (2013) 87–104. doi:10.1016/j.apenergy.2012.10.037.

[7] F. Oldewurtel, A. Parisio, C. N. Jones, M. Morari, D. Gyalistras, M. Gwerder, V. Stauch, B. Lehmann, K. Wirth, Energy efficient building climate control using stochastic model predictive control and weather predictions, in: Am. Control Conf., IEEE, 2010, pp. 5100–5105. doi:10.1109/ACC.2010.5530680.

[8] E. Vrettos, K. Lai, F. Oldewurtel, G. Andersson, Predictive Control of buildings for Demand Response with dynamic day-ahead and real-time prices, in: Eur. Control Conf., Zurich, Switzerland, 2013.

[9] S. Ganguly, N. C. Sahoo, D. Das, Recent advances on power distribution system planning: a state-of-the-art survey, Energy Syst. 4 (2013) 165–193. doi:10.1007/s12667-012-0073-x.

[10] P. S. Georgilakis, N. D. Hatziargyriou, A review of power distribution planning in the modern power systems era: Models, methods and future research, Electr. Power Syst. Res. 121 (2015) 89–100. doi:10.1016/j.epsr.2014.12.010.

[11] E. Lannoye, D. Flynn, M. O'Malley, The role of power system flexibility in generation planning, in: IEEE PES Gen. Meet., 2011. doi:10.1109/PES.2011.6039009.

[12] I. van Beuzekom, M. Gibescu, J. Slootweg, A review of multi-energy system planning and optimization tools for sustainable urban development, in: IEEE PowerTech, IEEE, Eindhoven, Netherlands, 2015. doi:10.1109/PTC.2015.7232360.

[13] S. Haffner, L. F. A. Pereira, L. A. Pereira, L. S. Barreto, Multistage model for distribution expansion planning with distributed generationpart i: Problem formulation, IEEE Transactions on Power Delivery 23 (2) (2008) 915–923.

[14] S. Troitzsch, S. Hanif, T. Hamacher, Distributed Robust Reserve Scheduling in Congested Distribution Systems, in: IEEE PES Gen. Meet., 2018. doi:10.1109/PESGM.2018.8586650.

[15] T. Logenthiran, D. Srinivasan, T. Z. Shun, Demand Side Management in Smart Grid Using Heuristic Optimization, IEEE Trans. Smart Grid 3 (3). doi:10.1109/TSG.2012.2195686.

[16] H. Wolisz, T. Schütz, T. Blanke, M. Hagenkamp, M. Kohrn, M. Wesseling, D. Müller, Cost optimal sizing of smart buildings' energy system components considering changing end-consumer electricity markets, Energy 137 (2017) 715–728. doi:10.1016/j.energy.2017.06.025.

[17] J. Kim, Y. Dvorkin, Peer-to-peer energy trading in distribution systems, arXiv Preprint (arXiv:1902.03940).

[18] A. Trpovski, D. Recalde, T. Hamacher, Synthetic Distribution Grid Generation Using Power System Planning: Case Study of Singapore, in: Int. Univ. Power Eng. Conf., 2018. doi:10.1109/UPEC.2018.8542054.

[19] C. S. Park, Contemporary Engineering Economics, 2010. doi:10.1038/151387c0.

[20] H. L. Willis, Power Distribution Planning Reference Book, CRC Press, 1997. doi:10.1201/9780824755386.

[21] Dena Deutsche Energie-Agentur, Ausbau- und Innovationsbedarf der Stromverteilnetze in Deutschland bis 2030 (2012).
URL https://www.dena.de/fileadmin/dena/Dokumente/Pdf/9100_dena-Verteilnetzstudie_Abschlussbericht.pdf

[22] EMA Energy Market Authority, Singapore Energy Statistics 2018 (2018).

[23] J. A. Fonseca, A. Schlueter, T.-A. Nguyen, F. Marechal, City Energy Analyst (CEA): Integrated framework for analysis and optimization of building energy systems in neighborhoods and city districts, Energy Build. 113 (2016) 202–226. doi:10.1016/J.ENBUILD.2015.11.055.

[24] BCA Building and Construction Authority, BCA Building Energy Benchmarking Report 2018 (2018).

[25] W. F. Holmgren, C. W. Hansen, M. A. Mikofski, pvlib python: a python package for modeling solar energy systems, J. Open Source Softw. 3 (29) (2018) 884. doi:10.21105/joss.00884.